Rotational sweepback of magnetic field lines in geometrical models of pulsar radio emission

J. Dyks[1] and Alice K. Harding

Laboratory for High Energy Astrophysics, Greenbelt, MD 20771, USA

`jinx@milkyway.gsfc.nasa.gov`, `harding@twinkie.gsfc.nasa.gov`

ABSTRACT

We study the rotational distortions of the vacuum dipole magnetic field in the context of geometrical models of the radio emission from pulsars. We find that at low altitudes the rotation deflects the local direction of the magnetic field by at most an angle of the order of $r_{\rm n}^2$, where $r_{\rm n} = r/R_{\rm lc}$, r is the radial distance of the radio emission and $R_{\rm lc}$ is the light cylinder radius. To the lowest (ie. second) order in $r_{\rm n}$, this distortion is symmetrical with respect to the plane containing the dipole axis and the rotation axis ($(\vec{\Omega}, \vec{\mu})$ plane). The lowest order distortion which is asymmetrical with respect to the $(\vec{\Omega}, \vec{\mu})$ plane is third order in $r_{\rm n}$. These results confirm the common assumption that the rotational sweepback has negligible effect on the position angle (PA) curve. We show, however, that the influence of the sweepback on the outer boundary of the open field line region (open volume) is a much larger effect, of the order of $r_{\rm n}^{1/2}$. The open volume is shifted backwards with respect to the rotation direction by an angle $\delta_{\rm ov} \sim 0.2 \sin\alpha \, r_{\rm n}^{1/2}$ where α is the dipole inclination with respect to the rotation axis. The associated phase shift of the pulse profile $\Delta\phi_{\rm ov} \sim 0.2 r_{\rm n}^{1/2}$ can easily exceed the shift due to combined effects of aberration and propagation time delays ($\approx 2r_{\rm n}$). This strongly affects the misalignment of the center of the PA curve and the center of the pulse profile, thereby modifying the delay-radius relation. Contrary to intuition, the effect of sweepback dominates over other effects when emission occurs at low altitudes. For $r_{\rm n} \lesssim 3 \cdot 10^{-3}$ the shift becomes negative, ie. the center of the position angle curve precedes the profile center. With the sweepback effect included, the modified delay-radius relation predicts larger emission radii and is in much better agreement with the other methods of determining $r_{\rm n}$.

Subject headings: pulsars: general — polarization — radiation mechanisms: non-thermal

---

[1] On leave from Nicolaus Copernicus Astronomical Center, Toruń, Poland

1. Introduction

There are independent observational arguments which imply that the pulsar radio emission occurs in a form of a narrow beam centered (or roughly centered) on the magnetic dipole axis. In many cases the position angle (PA) of the observed linearly polarized radiation changes its direction by nearly 180° when our line of sight crosses the radio beam (eg. Lyne & Manchester 1988). If associated with the direction of $\vec{B}$, this change of PA can be naturally interpreted as a result of our line of sight passing near the magnetic pole (Radhakrishnan & Cooke 1969). Moreover, the width ρ of the radio beam determined for different pulsars from the observed width of their radio pulse profiles scales with the rotation period P as the opening angle of the open field line region, ie. $\rho \propto P^{-1/2}$ (Rankin 1990; Rankin 1993).

It is commonly believed that the emission region associated with the beam does not extend beyond the region of open field lines (hereafter called "open volume") which cross the light cylinder of radius $R_{\mathrm{lc}} = c/\Omega$ (c is the speed of light and $\vec{\Omega} = \Omega \hat{z}$ is the angular velocity of pulsar rotation). The angular size of the open volume at (small) radial distance r is equal to $\theta_{\mathrm{ov}}^r \simeq (r/R_{\mathrm{lc}})^{1/2}$ and the cone formed by tangents to magnetic field lines at the rim of the open volume has angular radius of $\theta_{\mathrm{b}} \simeq 1.5\theta_{\mathrm{ov}}^r$. The radial distance of the emission region has not been established so far: both a high-altitude emission region extending over a small fraction of θ_{ov}^r, as well as a low-altitude emission region which fills in a much larger fraction of θ_{ov}^r may be responsible for the same shape of the radio beam.

The sweepback effect was first investigated in detail by Shitov (1983) who considered it to explain the observed dependence of radio luminosity of pulsars as a function of period. He estimated the magnitude of the rotational distortions of the magnetic field from the torque responsible for the observed slowing down of pulsars. He found that at moderate altitudes within the open volume, "near" the dipole axis, the direction of the distorted magnetic field deflects from the direction of the pure (ie. static shape) dipole barely by an angle

$$\delta_{\mathrm{sb}} \simeq 1.2 \left(\frac{r}{R_{\mathrm{lc}}} \right)^3 \sin^2 \alpha, \tag{1}$$

where α is the dipole inclination with respect to the rotation axis. Gil (1983) proposed the sweepback effect to explain why the separation between the main radio pulse and the interpulse observed in the profile of PSR B0950+08 is significantly different from 180°.

In 1985 Shitov incorporated the sweepback effect into the model of pulsar position angle curves proposed by Radhakrishnan & Cooke (1969) and showed that the sweepback results in a lag of the profile center (measured as the midpoint between the outer edges of the pulse profile) with respect to the center, or the "inflection point" of the position angle curve.

Shitov emphasized that the lag of the profile center was a sum of *two* effects: not only the center of the PA curve is shifted toward earlier phases (with respect to the nondistorted case) according to the eq. (1), but also the center of the open volume is displaced backwards, which contributes to the total effect.

In most of subsequent investigations, however, the sweepback has been neglected, mainly on the basis of eq. (1). Blaskiewicz et al. (1991, hereafter BCW91) proposed a relativistic model of pulsar polarization which took into account two important effects overlooked by Shitov: the presence of the corotational acceleration and the aberration effect. An excellent result of their work was the "delay-radius" relation, according to which the center of the PA curve *lags* the profile center by

$$\Delta\Phi_{BCW} \approx 4\frac{r}{R_{\mathrm{lc}}} \ \mathrm{rad}, \tag{2}$$

where r is the radial distance of the radio emission. With no dependence on viewing geometry parameters (like the dipole inclination α, or the viewing angle ζ_{obs} between the rotation axis and the observer's line of sight), their relation appears to provide a powerful method of determining r. Equally important, the delay-radius relation depends neither on the observed width of the pulse profile W nor on the separation between the conal components in the pulse profile. Therefore, the altitudes of radio emission provided by eq. (2) may serve to determine which magnetic field lines are associated with the outer edge of the profiles and which field lines correspond to the maxima of conal components (Mitra & Rankin 2002; Dyks et al. 2004a). Von Hoensbroech & Xilouris (1997) used the delay-radius relation to probe the radius-to-frequency mapping at high radio frequencies. Given that the method is based on a measurement of *tiny* shifts (of magnitude usually being a small fraction of one degree) between the centers of the PA curve and the profile, it is extremely sensitive to the assumed geometry of the magnetic field. The latter was taken to be a dipole of static shape, with no rotational distortions.

Gangadhara & Gupta (2001) proposed another relativistic method of estimating radio emission altitudes for pulsars with both core and conal components. By considering the effects of the aberration and the propagation time delays they showed that the core component lags in phase the midpoint between the maxima of conal components, if the core originates from lower altitudes than the cones, and if the cones are axially symmetric around the core in the reference frame corotating with the star (CF). Dyks et al. (2004a) revised their method and showed that the phase shift between the core component and the pairs of conal components is equal to

$$\Delta\phi_{DRH} \approx 2\frac{r}{R_{\mathrm{lc}}} \ \mathrm{rad} \tag{3}$$

which provides another method for determining r without information about viewing geometry (nor W). Dyks et al. (2004a) used the above relation, and the results of work by Gupta

& Gangadhara (2003) to calculate r for 6 pulsars with well defined core-cone systems. As in the case of the delay-radius relation, the above formula holds only for the magnetic field which is symmetrical about the $(\vec{\Omega}, \vec{\mu})$ plane (where $\vec{\mu}$ is the magnetic moment of the pulsar magnetic field), at least as long as one associates the assumed symmetry of the core-cone system with the geometry of the underlying magnetic field. Any asymmetrical (with respect to the $(\vec{\Omega}, \vec{\mu})$ plane) distortions of the magnetic field would pose a serious problems for the framework of the model leading to eq. (3). Again, based on eq. (1), any influence of the sweepback was neglected.

Given that the above-mentioned methods of determining r are so sensitive to the assumed symmetry of the magnetic field around $\vec{\mu}$, it is important to have the symmetry hypothesis well justified. It is also important to revise this assumption in view of the unacceptably low values of r which are often being derived with the BCW91 method: as found in BCW91, the "delay radii" r_{del} implied by their method (eq. 2) are often smaller (in some cases by an order of magnitude — see fig. 29 in BCW91) than the geometrical radii r_{geo} determined with the traditional geometrical method based on the measurement of profile widths (Cordes 1978; Gil & Kijak 1993; Kijak & Gil 2002). This poses a real problem for the BCW91 method, because the geometrical radii, in the absence of strong refraction effects (Lyubarski & Petrova 1998), should be considered as lower limits of r (Dyks et al. 2004a). Although one could explain this disagreement in many different ways (eg. underestimated theoretical width of the open volume, systematically overestimated impact angles and dipole inclinations α etc.), we show below that the rotational distortions of the static shape dipole may account for a large part of the discrepancies between r_{del} and r_{geo}.

Recently Kapoor & Shukre (2003) considered the aberration effect *and* the rotational sweepback to investigate the relative locations of core and cone components in the pulsar magnetosphere. Although included in the model, the sweepback is again estimated with the help of eq. (1). Being aware of the limitations of Shitov's estimate, the authors emphasized the need for derivation of a more advanced formula describing the rotational distortions of the magnetosphere. They noted that a proper derivation "should make use of at least the magnetic field given by the full Deutsch solution (Deutsch 1955)".

Such an estimate based on the Deutsch solution was done by Arendt & Eilek (1998), who concluded that the rotation distorts the magnetic field by a magnitude of the order of r/R_{lc}. Being much larger than the Shitov's estimate, this distortion would strongly affect results in BCW91, GG2001, Hibschman & Arons (2001, hereafter HA2001), and Dyks et al. (2004a). On the contrary, HA2001 noted that the leading terms in the difference between the Deutsch field and the rigidly rotating static-shape dipole are of the order of $(r/R_{\text{lc}})^2$. Recently, Mitra & Li (2004) emphasized that on the theoretical side there is a great need to

develop and understand the details of the sweepback effect.

In this paper we investigate the rotational distortions of the pulsar magnetic field assuming the approximation of the vacuum magnetosphere. The twofold nature of the sweepback, first noticed by Shitov (1983) will be highlighted, and limitations in applicability of eq. (1) will be clarified (Section 2). The significance of the sweepback for the relativistic model of pulsar polarization will appear to be much larger than previously thought, which will have serious consequencies for the delay-radius relation (eg. modification of eq. 2, Section 3).

2. The rotational distortions of the dipolar magnetic field

We follow previous investigators (Deutsch 1955; Shitov 1983; Barnard 1986; Romani & Yadigaroglu 1995, hereafter RY95; Cheng et al. 2000, hereafter CRZ2000) in assuming that the magnetic field surrounding the neutron star (NS) may be approximated by the vacuum rotating dipole. As in Barnard (1986), RY95, and CRZ2000, we assume that outside the NS the field is the same as of the star-centered *point* dipole, ie. we neglect the near-surface modifications of the magnetic field by the conducting sphere of the neutron star, derived by Deutsch (1955) (cf. Yadigaroglu 1997). Hereafter, the magnetic field will be called a "retarded dipole" and will be denoted by $\vec{B}_{\rm ret}$. In Appendix A we give the cartesian and the spherical components of $\vec{B}_{\rm ret}$ (eqs. A1 – A1 and A15 – A17, respectively).

We want to estimate how much the rotational sweepback distorts the magnetic field at low altitudes ($r \ll R_{\rm lc}$). One measure of this is the difference between the retarded magnetic field $\vec{B}_{\rm ret}$ and the magnetic field of the static-shape dipole $\vec{B}_{\rm st}$. The components of $\vec{B}_{\rm st}$ can be calculated with the help of eqs. (A15 – A17) taken in the limit of $r_{\rm n} \ll 1$ (ie. with the ratio $r_{\rm n}$ set equal to zero). We define the difference as:

$$\Delta \vec{B} = \vec{B}_{\rm ret} - \vec{B}_{\rm st}. \tag{4}$$

In all formulae we assume that both the retarded dipole and the static-shape dipole are associated with the same magnetic moment $\vec{\mu}$, which at the time $t = 0$ is in the $(\hat{x}, \hat{z})$ plane (time t is measured in the Lorentz frame in which the neutron star's center of mass is at rest). Thus, at any instant $\vec{\mu}_{\rm st} = \vec{\mu}_{\rm ret} = \vec{\mu}$, where

$$\vec{\mu} = \mu(\sin \alpha \cos \Omega t \; \hat{x} + \sin \alpha \sin \Omega t \; \hat{y} + \cos \alpha \; \hat{z}). \tag{5}$$

In the CF the components of $\vec{B}_{\rm ret}$ at any point which corotates with the magnetosphere do not depend on t (cf. eq. A4). Therefore, one is allowed to choose any convenient value. We take $t = 0$ ($\vec{\mu}$ in the $(\hat{x}, \hat{z})$ plane) and constrain our discussion to the half of the magnetosphere with positive values of x. The positive values of the y coordinate then correspond to the

leading part of the magnetosphere and the negative y correspond to the trailing part. In cartesian coordinates and for $t = 0$ the difference is:

$$\Delta B_x = \frac{\mu}{r^5} \sin \alpha \left[\frac{1}{2} \left(x^2 + r^2 \right) r_{\rm n}^2 + O(r_{\rm n}^4) \right] \tag{6}$$

$$\Delta B_y = \frac{\mu}{r^5} \sin \alpha \left[\frac{1}{2} \, xy \, r_{\rm n}^2 - \frac{2}{3} \, r^2 r_{\rm n}^3 + O(r_{\rm n}^4) \right] \tag{7}$$

$$\Delta B_z = \frac{\mu}{r^5} \sin \alpha \left[\frac{1}{2} \, xz \, r_{\rm n}^2 + O(r_{\rm n}^4) \right]. \tag{8}$$

In agreement with the remark of Hibschman & Arons (2001), the leading terms are second order in $r_{\rm n}$. The second order terms of ΔB_x and of ΔB_z do not depend on y. The second order term of ΔB_y is odd function of y ($\Delta B_y(y) = -\Delta B_y(-y) + O(r_{\rm n}^3)$). These features are important because the symmetry of any vector field $\vec{B} = (B_x, B_y, B_z)$ with respect to the $(\vec{\Omega}, \vec{\mu})$ plane requires the following relations to be satisfied: $B_x(x, y, z) = B_x(x, -y, z)$, $B_y(x, y, z) = -B_y(x, -y, z)$, and $B_z(x, y, z) = B_z(x, -y, z)$ (ie. the B_x and B_z components must be even, and the B_y component must be odd in y).

The angle κ between $\vec{B}_{\rm ret}$ and $\vec{B}_{\rm st}$, to the order $r_{\rm n}^3$, is given by:

$$\kappa \approx \left(f_1 r_{\rm n}^4 + f_2 r_{\rm n}^5 + f_3 r_{\rm n}^6 \right)^{1/2} \lesssim r_{\rm n}^2, \tag{9}$$

where the functions f_1, f_2, and f_3, given in Appendix A, depend on x, y, z, and on the inclination angle α (but not on $r_{\rm n}$) and in general have magnitude of the order of 1, except from special locations in the magnetosphere which we discuss below.

Thus, the rotation causes the magnetic field to deviate from $\vec{B}_{\rm st}$ by an angle which at most is second order in $r_{\rm n}$. Along the magnetic dipole axis[1] of an orthogonal rotator, however, (ie. for $\alpha = 90°$ and $(x, y, z) = (r, 0, 0)$), one obtains $f_1 = 0$, $f_2 = 0$ and $f_3 = 9^{-1}$ so that κ is third order in $r_{\rm n}$:

$$\kappa = \frac{1}{3} \, r_{\rm n}^3 \tag{10}$$

in partial agreement with the estimate of Shitov (1983). Beyond the orthogonal dipole axis, however, as well as at the dipole axis of non-orthogonal rotator, $f_1 \neq 0$ and κ may be much larger. On the $(\vec{\Omega}, \vec{\mu})$ plane $f_2 = 0$ (because $f_2 \propto y$, cf. eq. A5). Beyond the $(\vec{\Omega}, \vec{\mu})$ plane ($f_1 \neq 0$, $f_2 \neq 0$), the first two terms in eq. (9) dominate and give:

$$\kappa \simeq f_1^{1/2} r_{\rm n}^2 + \frac{f_2}{2 f_1^{1/2}} r_{\rm n}^3. \tag{11}$$

---

[1] By the "magnetic dipole axis" we understand the *straight* line containing the magnetic moment $\vec{\mu}$. In the case of the retarded dipole, the axis cannot be associated with any magnetic field line.

Let us estimate the angles κ_l and κ_t for two points $P_\mathrm{l}(x_\mathrm{l}, y_\mathrm{l}, z_\mathrm{l})$ and $P_\mathrm{t}(x_\mathrm{t}, y_\mathrm{t}, z_\mathrm{t})$ located symmetrically on both sides of the $(\vec{\Omega}, \vec{\mu})$ plane. Let us consider the particular case in which the points lie in the plane of rotational equator, close to the rim of the open volume of orthogonal rotator, ie. $x_\mathrm{l} = x_\mathrm{t} = r(1 - r_\mathrm{n})^{1/2}$, $y_\mathrm{l} = -y_\mathrm{t} = rr_\mathrm{n}^{1/2}$, and $z_\mathrm{l} = z_\mathrm{t} = 0$, with the positive value of the y coordinate corresponding to the point P_l on the leading side of the open volume, and the negative y for the trailing point P_t (cf. Fig. 1). Then eq. (A5) gives $f_1 = 4^{-1}r_\mathrm{n}$, $f_2 = \pm 3^{-1}r_\mathrm{n}^{1/2}$, which results in $\kappa_\mathrm{l} \approx 2^{-1}r_\mathrm{n}^{5/2} + 3^{-1}r_\mathrm{n}^3$ and $\kappa_\mathrm{t} \approx 2^{-1}r_\mathrm{n}^{5/2} - 3^{-1}r_\mathrm{n}^3$. Both angles are considerably larger than the distortion of the magnetic axis given by eq. (10).

Eqs. (6 – 8) imply, however, that up to the second order in r_n, the rotational distortion of $\vec{B}_\mathrm{st}$ *is symmetrical* with respect to the $(\vec{\Omega}, \vec{\mu})$ plane (because ΔB_x is even, and the leading term of ΔB_y is odd in y). This (approximate) symmetry, shown in Fig. 1, implies that *beyond the dipole axis of the orthogonal rotator* the angle κ between $\vec{B}_\mathrm{ret}$ and $\vec{B}_\mathrm{st}$ provides no information about the magnitude of the asymmetry of $\vec{B}_\mathrm{ret}$ with respect to the $(\vec{\Omega}, \vec{\mu})$ plane.

To estimate the asymmetry for points located beyond the $(\vec{\Omega}, \vec{\mu})$ plane, one must therefore use the difference between azimuths of $\vec{B}_\mathrm{ret}$ at the points P_l and P_t:

$$\Delta\phi_\mathrm{l-t} \equiv |\phi_\mathrm{t}| - \phi_\mathrm{l} \approx \left| \frac{B_{\mathrm{ret},y}(P_\mathrm{t})}{B_{\mathrm{ret},x}(P_\mathrm{t})} \right| - \frac{B_{\mathrm{ret},y}(P_\mathrm{l})}{B_{\mathrm{ret},x}(P_\mathrm{l})} \approx \frac{4}{3} \frac{\mu}{r^3} \frac{\sin\alpha}{B_{\mathrm{st},x}} r_\mathrm{n}^3, \tag{12}$$

where ϕ_l is the azimuth of $\vec{B}_\mathrm{ret}$ at the point $P_\mathrm{l}(x_\mathrm{l}, y_\mathrm{l}, z_\mathrm{l})$, ϕ_t is the azimuth of $\vec{B}_\mathrm{ret}$ at $P_\mathrm{t}(x_\mathrm{l}, -y_\mathrm{l}, z_\mathrm{l})$ (cf. Fig. 1), and

$$B_{\mathrm{st},x} = \frac{\mu}{r^3} \left[3\frac{x}{r}\frac{z}{r} \cos\alpha + \left(3\frac{x^2}{r^2} - 1 \right) \sin\alpha \right]. \tag{13}$$

Equation (12) clearly demonstrates that $\Delta\phi_\mathrm{l-t}$ is third order in r_n, ie. the rotation induces the asymmetry of $\vec{B}_\mathrm{ret}$ with respect to the $(\vec{\Omega}, \vec{\mu})$ plane with magnitude of the order of r_n^3. Equation (12) is not useful in the immediate vicinity of the $(\vec{\Omega}, \vec{\mu})$ plane (nor at the plane itself), because ϕ_l changes sign to negative (ie. $\vec{B}_\mathrm{ret}$ is parallel to the $(\vec{\Omega}, \vec{\mu})$ plane) for locations with the tiny azimuth

$$\phi_\| \approx \frac{y}{x} \approx \frac{2}{9} r_\mathrm{n}^3 \left(\frac{x}{r}\frac{z}{r}\frac{1}{\tan\alpha} + \frac{x^2}{r^2} \right)^{-1} \simeq \frac{2}{9} r_\mathrm{n}^3 \tag{14}$$

(ie. within a narrow region on the leading side of the $(\vec{\Omega}, \vec{\mu})$ plane $B_{\mathrm{ret},y} < 0$ and eq. (12) gives a sum rather than a difference of azimuths). To estimate the asymmetry on the $(\vec{\Omega}, \vec{\mu})$ plane one can use the difference of azimuths of $\vec{B}_\mathrm{st}$ and $\vec{B}_\mathrm{ret}$ at a given (the same) point:

$$\Delta\phi_\mathrm{s-r} \equiv \phi_\mathrm{st} - \phi_\mathrm{ret} \approx \frac{B_{\mathrm{st},y}}{B_{\mathrm{st},x}} - \frac{B_{\mathrm{ret},y}}{B_{\mathrm{ret},x}} \approx f_4 r_\mathrm{n}^2 + \frac{2}{3} \frac{\mu}{r^3} \frac{\sin\alpha}{B_{\mathrm{st},x}} r_\mathrm{n}^3, \tag{15}$$

where the function $f_4(x, y, z, \alpha)$ is given in Appendix A (eq. A14). Beyond the $(\vec{\Omega}, \vec{\mu})$ plane the first term in this equation dominates (ie. $\Delta\phi_{s-r} \simeq f_4 r_n^2$) but it is symmetrical with respect to the $(\vec{\Omega}, \vec{\mu})$ plane (ie. odd in y, $f_4 \propto y$). Therefore, just like κ given by eq. (9), $\Delta\phi_{s-r}$ provides no estimate of the rotational asymmetry there. On the $(\vec{\Omega}, \vec{\mu})$ plane $f_4 = 0$ and $\Delta\phi_{s-r}$ does measure the asymmetry which is of the order of r_n^3. Along the dipole axis $B_{st,x} = 2\mu \sin\alpha/r^3$ so that $\Delta\phi_{s-r} \simeq 3^{-1} r_n^3$, independent of α.

Eqs. (9), (12), and (15) can be summarized as follows: the rotation changes the components and the direction of the dipolar magnetic field by $\sim r_n^2$. To the order of r_n^2 this change, however, is symmetrical with respect to the $(\vec{\Omega}, \vec{\mu})$ plane. The *asymmetrical* change of the magnetic field direction has much smaller magnitude of the order of r_n^3 and is given by the second term of eq. (15).

An immediate consequence of eq. (9) is that with accuracy of the order of r_n, the rotation does not affect the shape of the position angle curve which depends on the *local* direction of $\vec{B}_{ret}$. This allows one to neglect the influence of the sweepback *on the position angle curve* as long as only the first order effects in r_n are considered. Given the tiny magnitude of the rotational asymmetry as defined by eq. (12), investigators often neglect its influence on the shape of the pulse profile as well (eg. BCW91, GG2001, HA2001). As we show below, this is not justified.

2.1. The rotational distortions of the open field line region

In the method of BCW91, the center of the pulse profile is most efficiently measured as a midpoint between the *outer edges* of the profile. Therefore, the method is based on the assumption that the *outer boundary* of the open volume is symmetrical with respect to the $(\vec{\Omega}, \vec{\mu})$ plane. Due to the complexity of the magnetic field lines in the retarded case, we determine the outer boundary of the open volume numerically, by finding the magnetic field lines which are tangent to the light cylinder. The method is described in detail in Dyks et al. (2004b).

Thick solid lines in Fig. 2 present the transverse shape of the open volume at low altitudes ($r_n \ll 1$), calculated for the retarded magnetic field $\vec{B}_{ret}$. More precisely, they represent the crossection of the outer boundary of the open volume with a sphere of radius $r = 0.01 R_{lc}$ centered at the neutron star. Different panels correspond to different dipole inclinations α. The magnetic moment $\vec{\mu}$ in all panels emerges perpendicularly from the page at the point $(x_m, y_m) = (0, 0)$. The thin circles have radius equal to $r\theta_{ov}^r = r r_n^{1/2}$, and are centered at the $(0, 0)$ point to guide the eye in assessing the asymmetry of the open volume

around $\vec{\mu}$. Given the small difference between the local direction of $\vec{B}_{\mathrm{ret}}$ and $\vec{B}_{\mathrm{st}}$ (eq. 9), one may regard each panel to be permeated by the magnetic field of the *static* dipole with the *straight* magnetic field line emerging from the $(0,0)$ point toward the reader. The field is symmetric relative to the $(\vec{\Omega}, \vec{\mu})$ plane, ie. with respect to the vertical line of $x_{\mathrm{m}} = 0$ (to be imagined in each panel of Fig. 2). In the course of corotation, the contours of the open volume outer boundary move to the left in Fig. 2, ie. $x_{\mathrm{m}} < 0$ correspond to the leading, and $x_{\mathrm{m}} > 0$ to the trailing side. An observer's line of sight cuts the contours horizontally, moving left to right.[2]

The following important conclusions can be drawn from Fig. 2: 1) the open volume is strongly asymmetric with respect to the $(\vec{\Omega}, \vec{\mu})$ plane; 2) the magnitude of the asymmetry depends on y_{m} and thus on the impact angle β; 3) regardless of the value of β the pulse window associated with the outer boundary of the open volume is always shifted backwards, ie. toward later phases; 4) the magnitude of this rotational asymmetry is very large, much larger than the local changes of the direction of the magnetic field caused by the rotation (eq. 9), and even larger than r_{n} (for large α the "retarded contours" are (on average) shifted toward later phases by $\sim 0.2\theta_{\mathrm{ov}}^{r} = 0.2 r_{\mathrm{n}}^{1/2} = 0.02$ to be compared with $r_{\mathrm{n}} = 0.01$).

This numerical result implies that none of the previous estimates (neither eqs. 12, 15, nor the Shitov's formula 1) provide a reliable measure of the rotational distortion of the *open volume* shape. The reason for this is that the boundary of the open volume is not only determined by the local (ie. low-altitude) direction of $\vec{B}_{\mathrm{ret}}$, but also (and most importantly) by the geometry of $\vec{B}_{\mathrm{ret}}$ near the light cylinder, where $r_{\mathrm{n}} \sim 1$. At R_{lc} all "higher order" effects become comparable in magnitude to the lowest order effects, in the sense that $r_{\mathrm{n}}^{m} \sim 1$ for any m. With the strength of the rotational distortions being very large at R_{lc}, a very different set of magnetic field lines is picked up as the last open field lines which form the boundary of the open volume. This "retarded" boundary is highly asymmetrical with respect to the $(\vec{\Omega}, \vec{\mu})$

---

[2]Note that our Fig. 2, calculated for $t = 0$ in eqs. (A1 – A3), differs significantly from analogous figures shown in Arendt & Eilek (1998) and in CRZ2000. The location of the *retarded* polar caps in their figures corresponds to the magnetic moment $\vec{\mu}$ rotated by the angle $\Omega R_{\mathrm{ns}}/c$ with respect to the $(\hat{x}, \hat{z})$ plane (ie. they assume $t = R_{\mathrm{ns}}/c$ in eqs. A1 –A3). At the same time, however, they assume $t = 0$ ($\vec{\mu}$ in $(\hat{x}, \hat{z})$ plane) to position the polar caps for the *static* case. Therefore, their figures do not inform us what is the relative position of the static and retarded caps in phase - only the caps' shapes can be compared. (To enable this, their retarded caps would have to be derotated by $\Omega R_{\mathrm{ns}}/c$ with respect to the static caps.) Also, note that the components of the magnetic field for the static-shape dipole given in CRZ2000 (eqs. A1–A3 therein) are for $t = 0$ whereas the components for the retarded dipole (eqs. B2-B4 in CRZ2000) are for $t = R_{\mathrm{ns}}/R_{\mathrm{lc}}$. Their difference does not give eqs. (6 – 8): by overlooking this misalignment of the dipoles Arendt & Eilek (1998) incorrectly estimated that the rotational distortions of the magnetic field are of the order of r_{n}. For moderate dipole inclinations ($\alpha \sim 40° - 50°$) the contours shown in Fig. 2 possess a notch rather than a discontinuous "glitch" suggested in Arendt & Eilek (1998) (see Dyks et al. 2004b for details).

plane (Fig. 2), and the magnitude of this asymmetry has little to do with the low-altitude rotational distortions as estimated with eqs. (12), (15) and with Shitov's formula, because *the low-altitude crossection of the open volume boundary is an image of the strong near-$R_{\rm lc}$ distortions projected through the continuity of the magnetic field lines.* Hereafter, we will refer to the asymmetrical distortion of the open volume with the terms "backward shift" or "displacement" of open volume.

Another numerical result is that the contours shown in Fig. 2 are (with high accuracy) the same for any radial distance $r_{\rm n}$, as long as $r_{\rm n} \ll 1$, and as long as their size is normalized by $r\theta^r_{\rm ov} = rr^{1/2}_{\rm n}$, as in Fig. 2. Contours calculated eg. for $r_{\rm n} = 10^{-3}$ or $r_{\rm n} = 0.1$ look exactly the same as those shown in Fig. 2. This means that for $r_{\rm n} \ll 1$ the overall (ie. averaged over the impact angle β) angular displacement of the open volume $\delta_{\rm ov}$ is a fixed fraction of the angular radius of the open volume $\theta^r_{\rm ov}$:

$$\delta_{\rm ov} \simeq a\theta^r_{\rm ov} \approx ar^{1/2}_{\rm n} \qquad (16)$$

with $a \simeq 0.2 \sin\alpha$. The dependence $a \propto \sin\alpha$ has been determined by noting that $\delta_{\rm ov}$ (measured from the star center) decreases with α (Fig. 2), whereas the corresponding phase shift $\Delta\phi_{\rm ov} \approx \delta_{\rm ov}/\sin\alpha$ of the pulse profile does not (cf. Fig. 3, the discussion in Section 3.1, as well as eq. A8 in Dyks et al. 2004a).

Equation (16) implies that the rotational displacement of the open volume has magnitude comparable to the combined effects of aberration and propagation time delays (hereafter APT effects, of magnitude $2r_{\rm n}$, cf. Dyks et al. 2004a) for $r_{\rm n} \sim a^2/4 \sim 0.01$, which is quite typical estimate of radio emission altitudes (eg. Gupta & Gangadhara 2003; Kijak & Gil 2003). For $r_{\rm n} \ll 0.01$ the backward shift of the open volume dominates over the APT effects. For $r_{\rm n} \gg 0.01$ the APT effects dominate over the open volume shift.

2.2. Twofold nature of the rotational distortions

We find, therefore, that the nature of the rotational distortions at low altitude is twofold: in addition to the famous (but negligible) asymmetrical distortion of the local magnetic field direction (of magnitude $\sim r^3_{\rm n}$, eqs. 12 and 15) the rotation shifts the open volume backward by a much larger amount of $\sim r^{1/2}_{\rm n}$. The low-altitude shift of the open volume is not caused by the distortions of the shape of magnetic field lines *at low altitudes* — locally their shapes are pretty much the same as those of the static dipole. It is due to the strong near-$R_{\rm lc}$ distortions: magnetic field lines which are picked up as the last open magnetic field lines by the tangency condition at the light cylinder are located asymmetrically with respect to the $(\vec{\Omega}, \vec{\mu})$ plane. The near symmetry of the field lines at low altitudes does not imply similar

symmetry of the open volume, because its shape is also governed by the geometry of the field near R_{lc}.

Although Shitov (1985) in his analysis of the phase shift between the pulse profile center and the center of the position angle curve neglected the APT effects, he did include the backward displacement of the open volume and did emphasize the twofold nature of the rotational distortions (cf. his fig. 2). However, he has not provided any simple estimate of the open volume displacement (like eq. 16). Therefore, in most studies following his work only the tiny local deflection of $\vec{B}$ has been considered (eqs. 12, 15 and Shitov's estimate), usually only to infer that the rotational distortions are negligible in generation of any asymmetry in a pulse profile.

3. Implications for the relativistic model of pulsar polarization

Implications of the rotational displacement of the open volume for the relativistic model of pulsar polarization are profound, because this effect is *lower* order ($\sim r_n^{1/2}$, eq. 16) than the effects considered so far (aberration $\sim r_n$, propagation time delays $\sim r_n$). Although the PA curve is practically unaffected, the center of the pulse profile to which the PA refers is considerably displaced.

Let us define a phase zero as a moment at which an observer detects a light signal emitted from the neutron star center when $\vec{\mu}$ was in the $(\vec{\Omega}, \vec{\mu})$ plane. As discussed in Dyks et al. 2004a, the total phase shift $\Delta\Phi$ between the center of the position angle curve and the pulse profile center can then be separated into two components: the shift of the center of the PA curve by $\Delta\phi_{PA} \approx 2r_n$ towards later phases with respect to the zero phase, and the shift of the pulse profile center toward earlier phases by $\Delta\phi_{pf}$ with respect to the zero phase. Had the boundary of the open volume been symmetrical with respect to the $(\vec{\Omega}, \vec{\mu})$ plane (as in the case of the static-shape dipole) the profile center would be shifted forward in phase by $\Delta\phi_{pf} \approx -2r_n$ which would result in the total shift of $4r_n$ as initially predicted by BCW91. Due to the backward displacement of the open volume given by eq. (16), however, the forward profile shift is decreased by $\Delta\phi_{ov} \equiv Fr_n^{1/2}$ (with $F \sim a/\sin\alpha$) so that $\Delta\phi_{pf} = -(2r_n - Fr_n^{1/2})$.

Therefore, the delay-radius relation of BCW91 (eq. 2) becomes:

$$\Delta\Phi \equiv \Delta\phi_{PA} + (-\Delta\phi_{pf}) \approx 2r_n + (2r_n - Fr_n^{1/2}) \qquad (17)$$

with F in general being a complicated function of α, ζ and r_n. The complicated form of F results from the complicated shape of the open volume boundary (Fig. 2) which implies nontrivial dependence of F on the impact angle and thereby on ζ. Since the sign of the impact angle $\beta = \zeta - \alpha$ provides no information about whether the viewing trajectory is

poleward or equatorward (in the sense defined in Everett & Weisberg 2001) hereafter we will use the angle

$$\beta_{\mathrm{x}} = \left\{ \begin{array}{ll} \beta, & \text{if } \alpha \leq 90° \\ -\beta, & \text{if } \alpha > 90° \end{array} \right. \tag{18}$$

which is negative/positive for poleward/equatorward viewing geometry regardless of whether $\alpha > 90°$ or not. Changes of F as a function of $\tau \equiv \beta_{\mathrm{x}}/\theta_{\mathrm{b}} \approx \beta_{\mathrm{x}}/(1.5 r_{\mathrm{n}}^{1/2})$ are illustrated in Fig. 3 for the same angles α as those in Fig. 2. The functions $F(\tau)$ were calculated for $r_{\mathrm{n}} = 0.01$, however, they change little with r_{n}, as long as $r_{\mathrm{n}} \ll 1$. Fig. 3 shows that F is confined to the rather limited range of $0.1 - 0.4$ for any combinations of α and ζ. Also, F is always positive which implies that the displacement of the open volume results in a smaller phase shift $\Delta\Phi$ than predicted by the original delay-radius relation (eq. 2). The radio emission radii provided by the original delay-radius relation are therefore underestimated by a factor which may be very large for some parameters.

3.1. The misalignment formula

The delay-radius relation which includes the rotational distortions of the open volume (in the vacuum approximation) becomes:

$$\Delta\Phi \approx 4 r_{\mathrm{n}} - F(\alpha, \zeta, r_{\mathrm{n}}) \, r_{\mathrm{n}}^{1/2} \tag{19}$$

and it is plotted in Fig. 4 for a few values of F equal to 0.1, 0.2, 0.3, and 0.4 (solid, dotted, dashed, and dot-dashed curve, respectively). (For convenience, $\Delta\Phi$ on the vertical axis is in degrees, whereas eq. 19 gives $\Delta\Phi$ in radians.) The thick dashed line presents the original delay-radius relation of eq. 2. For $r_{\mathrm{n}} < F^2/16$ (eg. for $r_{\mathrm{n}} < 10^{-2}$ for $F = 0.4$, dot-dashed line), ie. for small emission radii, the phase shift $\Delta\Phi$ becomes negative (ie. the center of the PA curve *precedes* in phase the profile center), which is a new feature in comparison with the original delay-radius relation which always predicted the *delay* of the PA curve with respect to the profile. Since eq. (19) predicts that the center of the PA curve may either precede or lag the center of the profile, it will be referred to as the "misalignment" formula. For large radii $r_{\mathrm{n}} \gtrsim 10^{-2}$ the formula always predicts positive $\Delta\Phi$ and, for increasing r_{n}, *slowly* converges to the original delay-radius relation.

For any $\Delta\Phi$, the radio emission radii estimated with the original delay-radius relation underestimate those implied by eq. (19) (cf. Fig. 4). For $\Delta\Phi \sim 1°$, the delay-radius relation underestimates r given by eq. (19) by a factor of $1.5 - 4$ (depending on F). For $\Delta\Phi \approx 0.3°$, $0.1°$, and $0.01°$ the underestimate factor is in the range of $2 - 9$, $3 - 22$, and $16 - 220$, respectively. For $\Delta\Phi \approx 0$ the underestimation factor is formally infinite. In the absence

of effects described in Section 4, the negative values of the shift $\Delta\Phi$ cannot be lower than $-F^2/16 \geq -0.57°$.

Unlike the original delay-radius relation, the misalignment formula predicts that the implied emission radii depend on the viewing geometry (especially on β_x) and that this dependence cannot be separated from the dependence on r_n: even for fixed α and β_x, when the line of sight probes the magnetosphere deeper and deeper (ie. when r_n decreases in Fig. 4), the absolute value of the parameter $\tau \equiv \beta_x/(1.5 r_n^{1/2})$ increases — the line of sight cuts through the open volume more peripherally. This departure from $\tau = 0$ in Fig. 3 implies that the value of F changes (sometimes abruptly) with varying r_n, ie. for fixed α and β_x the value of F is not fixed — it depends on r_n.

The complicated behaviour of the misalignment formula (19), is exemplified in Fig. 5, which presents $\Delta\Phi$ as a function of r_n calculated numerically for $\alpha = 45°$ and three values of $\zeta_{obs} = 43$, 45, and 47° (circles, squares, and crosses, respectively). For large r_n (and so for large $\Delta\Phi$) the line of sight crosses the open volume nearly centrally ($\beta_x \ll 1.5\theta_{ov}^r$, $\tau \simeq 0$), so that $F \simeq 0.1$, regardless of the value of ζ_{obs} and α (cf. Fig. 3). Therefore, all the three numerical solutions stay close to the analytical solution for $F = 0.1$ (thin solid line). For smaller r_n, (and $\Delta\Phi \lesssim 1°$), the numerical results diverge from each other: the case of $\zeta_{obs} = \alpha = 45°$ (squares) remains close to the analytical solution with $F \simeq 0.1$ (it follows eq. (19) with $F \approx 1.07$), because the parameter $\tau \propto \beta_x$ is fixed and equal to zero. In the case of $\zeta_{obs} = 47°$ (equatorward viewing, crosses in Fig. 5), the parameter τ increases with decreasing r_n because the line of sight traverses more peripherally through the open volume. As can be inferred from Fig. 3 (panel for $\alpha = 45°$) this makes F increase through 0.2 up to ~ 0.26 for $\tau \simeq 1$, and accordingly, the numerical solution in Fig. 5 crosses the dotted line for $F = 0.2$ and approaches the vicinity of the dashed line for $F = 0.3$. At $\log r_n \simeq -3.33$ the line of sight just grazes the outer boundary of the open volume ($\tau \simeq 1.08$). At smaller radial distances the line of sight does not penetrate the open volume. In the poleward case of $\zeta_{obs} = 43°$ (circles in Fig. 5), τ becomes more negative with decreasing r_n. Since the backward displacement of the open volume is stronger on its poleward side (cf. Figs. 2 and 3) the solution crosses the analytical curve for $F = 0.2$ (dotted line in Fig. 5) earlier than in the equatorward case (ie. at smaller $|\tau|$). At $\log r_n \simeq -2.43$, the line of sight starts to cut the radiation beam *above* the notch visible in Fig. 2. This results in a discontinuous increase of F from ~ 0.25 up to ~ 0.39 (Fig. 3). Therefore, the numerical solution jumps to the vicinity of the dot-dashed line of $F = 0.4$ (Fig. 5). For more peripheral traverses (ie. for smaller r_n and more negative τ), F changes little between 0.39 and 0.35, and the numerical solution departs only slightly from the $F = 0.4$ curve. For $\log r_n \lesssim -3.25$ the line of sight misses the open volume. This minimum value of $\log r_n$ differs slightly from the one for $\beta_x = +2°$ (crosses) because in addition to the backward displacement,

the open volume is also slightly shifted (with respect to $\vec{\mu}$) towards the rotational equator (ie. downwards in Fig. 2).

3.2. Determination of emission radius

The above-described complicated form of the function $\Delta\Phi(r_\mathrm{n}, \alpha, \zeta_\mathrm{obs})$ does not allow an easy determination of r_n. Numerical determination of r_n based on the known values of $\Delta\Phi$, α, and ζ_obs requires rather complicated calculations. Therefore, below we discuss the particular cases when easy derivation of r_n is possible and then we propose a procedure, which allows the possible range of r_n to be constrained in a general case of arbitrary viewing geometry.

As can be inferred from Fig. 3, the value of F is (nearly) fixed and close to 0.1 whenever $|\tau| \ll 0.4$, ie. whenever $|\beta| \ll 0.6 r_\mathrm{n}^{1/2}$. The condition is fulfilled for any r_n and α when $\beta \approx 0$ ($\alpha \approx \zeta_\mathrm{obs}$, squares in Fig. 5). The other case when the condition is fulfilled is when the measured shift between the position angle center and the profile center is large ($\gtrsim 1°$) and the impact angle $|\beta|$ is small: the radiation comes then from high-altitudes, where $\theta_\mathrm{ov}^r \gg |\beta|$. This is why all numerical results shown in Fig. 5 approach the solid line of $F = 0.1$ when $\Delta\Phi$ increases above $1°$.

When F is fixed (like in the above-described cases), the equation (19) can be inverted to obtain analytical solutions for $r_\mathrm{n}(\Delta\Phi)$:

$$r_\mathrm{n} = 32^{-1} \left[8\Delta\Phi + F^2 + k \left(16\Delta\Phi F^2 + F^4 \right)^{1/2} \right] \tag{20}$$

where the parameter $k = 1$ for $\Delta\Phi > 0$ whereas $k = \pm 1$ for $\Delta\Phi < 0$. Thus, the solution for r_n is unique if $\Delta\Phi$ is positive, whereas for the negative $\Delta\Phi$ *two* solutions are possible. One can attempt to reject the smaller one of these solutions by using the theoretical constraints:

$$r_\mathrm{n} \geq \frac{R_\mathrm{ns}}{R_\mathrm{lc}} \quad \text{and} \quad r_\mathrm{n} \geq \frac{4}{9} \beta^2. \tag{21}$$

The second constraint holds when the emission is limited to the open volume.[3] In the two above-mentioned cases (when $\beta \approx 0$ or $\Delta\Phi \gtrsim 1°$), one can directly use eq. (20) with $F = 0.1$ to calculate r_n.

---

[3]In application to the retarded dipole field this condition is approximate, not exact. Therefore, the minimum values of $\log r_\mathrm{n}$ determined numerically for $\beta = \pm 2°$ in Fig. 5 (circles and crosses) differ slightly from -3.266.

In a general case (including the common case when $\beta \neq 0$ and the shift is small) one can constrain r_n to a degree which depends on the information available. Without the knowledge of α and β one can obtain a *rough* estimate of r_n based on the measured shift $\Delta\Phi$ by assuming some averaged, fixed value of F in eq. 19 (eg. $F = 0.2$). This is equivalent to igoring the dependence of $F(\alpha, \tau)$ shown in Fig. 3. For $r_n \leq 10^{-2}$ this may give results wrong by as much as an order of magnitude due to the large horizontal spread of r_n as allowed by the range of F (Fig. 4).

Therefore, a better approach is to use the following two-step procedure: 1) Using eq. (20) one can calculate the *range* of r_n allowed by $0.1 \leq F \leq 0.4$ and by the conditions (21). Or, one can draw a horizontal line in Fig. 4 to determine graphically the range of r_n allowed by the range of F (the measurement error of $\Delta\Phi$ can easily be taken into account by drawing a horizontal strip instead of the line). For $-0.0358° \leq \Delta\Phi < 0$, two ranges of r_n are allowed and again the constraints (21) may be used to try to reject the lower range. For $-0.573° \leq \Delta\Phi < -0.0358°$, the allowed range of r_n is between $r_n^{\min}$ and $r_n^{\max}$ where $r_n^{\min}$ is given by eq. (20) with $k = -1$ and $F = 0.4$ and $r_n^{\max}$ by eq. (20) with $k = +1$ and the same value of $F = 0.4$.

2) With the knowledge of α and β one can more tightly constrain the allowed range of r_n by calculating $\tau_{\min} = \tau(r_n^{\max})$ and $\tau_{\max} = \tau(r_n^{\min})$ where $r_n^{\min}$ and $r_n^{\max}$ were determined in the previous step. Then, from Fig. 3, using the appropriate panel, one can determine the narrower range of $(F_{\min}, F_{\max})$ corresponding to the range of $(\tau_{\min}, \tau_{\max})$. Then, one returns to the step 2) in which the tightened range $(F_{\min}, F_{\max})$ must be used instead of the original range of $(0.1, 0.4)$.

If the sign of β is unknown, the step 2) may (but does not have to) give two ranges of r_n. If the sign is positive (equatorward viewing) the range of F considered in the step 1) may be narrowed to $0.1 - 0.25$ (Fig. 3).

As an example we apply the method to PSR B0301+19 and B0525+21. In the case of B0301+19 ($P = 1.38$ s), BCW91 find $\Delta\Phi = 0.2 \pm 0.1°$ at 1.4 GHz. The range of r_n for F between 0.1 and 0.4 is $(r_n^{\min}, r_n^{\max}) = (2.0 \cdot 10^{-3}, 1.2 \cdot 10^{-2})$, or, if we allow for the error of $\Delta\Phi$, the range becomes $(1.4 \cdot 10^{-3}, 1.25 \cdot 10^{-2})$ (step 1). For $\beta_x = -0.96 \pm 0.63°$ (Everett & Weisberg 2001, hereafter EW2001) Fig. 3 gives $(\tau_{\min}, \tau_{\max}) = (-0.3, -0.1)$ (with the error of $\Delta\Phi$ included) or $(\tau_{\min}, \tau_{\max}) = (-0.5, -0.03)$ (including also the error of β_x). EW2001 derived $\alpha = 162.4 \pm 11.8°$, so that $\pi - \alpha \approx 17.6°$ and we may use the panel of Fig. 3 for $\alpha = 20°$ to constrain the range of F to $(F_{\min}, F_{\max}) = (0.14, 0.22)$. This new range of F translates to $(r_n^{\min}, r_n^{\max}) = (2.7 \cdot 10^{-3}, 4.6 \cdot 10^{-3})$ if the error of $\Delta\Phi$ is neglected (and the error of β_x is included). Taking into account the error of $\Delta\Phi$ one finally obtains $(r_n^{\min}, r_n^{\max}) = (2.0 \cdot 10^{-3}, 5.3 \cdot 10^{-3})$. None of the constraints (21) narrows this range. This result is in agreement with the condition $r_n \geq r_{geo}/R_{lc}$. For the observed pulse width

$W \approx 15.9°$ (BCW91) and for α and β cited above, one finds $r_{\mathrm{geo}}/R_{\mathrm{lc}} \approx 1.3 \cdot 10^{-3}$. Our value of $r_{\mathrm{n}} = (2 - 5.3) \cdot 10^{-3}$ implies that the emission associated with the profile edge must originate from magnetic field lines with magnetic colatitude $\theta_{\mathrm{m}} \approx (0.5 - 0.8)\theta_{\mathrm{ov}}^r$. The original delay-radius relation gives $r_{\mathrm{n}} \approx 9 \cdot 10^{-4}$ (3 times smaller) which results in $\theta_{\mathrm{m}}/\theta_{\mathrm{ov}}^r > 1$ (emission from the region of closed field lines).

In the case of B0525+21 ($P = 3.74$ s), BCW91 find $\Delta\Phi = 0.3 \pm 0.1°$ at 430 MHz. At this value of $\Delta\Phi$ the range of $F = 0.1 - 0.4$ translates into $(r_{\mathrm{n}}^{\mathrm{min}}, r_{\mathrm{n}}^{\mathrm{max}}) = (2.6 \cdot 10^{-3}, 1.2 \cdot 10^{-2})$ or into $(2 \cdot 10^{-3}, 1.3 \cdot 10^{-2})$ if the error of $\Delta\Phi$ is included. For $\beta_{\mathrm{x}} = 1.5 \pm 0.08°$ (EW2001) we find $(\tau_{\mathrm{min}}, \tau_{\mathrm{max}}) = (0.15, 0.39)$. EW2001 suggest $\pi - \alpha = 63.2°$ which implies that $F \simeq 0.1$ (Fig. 3, panel for $\alpha = 60°$). Using this value in eq. (19) one finds that $r_{\mathrm{n}} = (2.6 \pm 0.6) \cdot 10^{-3}$ which is two times larger than the value predicted by the original delay-radius relation (eq. 2). However, the value is still six times smaller than $r_{\mathrm{geo}}/R_{\mathrm{lc}} = 1.7 \cdot 10^{-2}$ (calculated for $W = 20.4°$) and implies that the emission at the profile edge comes from magnetic field lines with colatitudes $\theta_{\mathrm{m}} = (2.4 - 3.0)\theta_{\mathrm{ov}}^r$, ie. from the closed line region. A large part of this discrepancy can be removed by considering different emission altitudes across the pulse profile.

4. Altitude-dependent position angle swing

When different parts of the pulse profile originate from different altitudes, the PA curve can no longer be described by the standard equation of Radhakrishnan & Cooke (1969). The simple analytical equation for the altitude-dependent PA swing is given in eq. (16) of BCW91. The formula predicts that if the radial distance r of the radio emission is uniform across the pulse profile, the entire PA curve is shifted rightwards (toward later phases) by $2r$ with respect to the zero phase. This effect is illustrated in Fig. 6: The thin solid line with dots is the PA curve for the fixed emission altitude of $r_{\mathrm{n}} = 10^{-2}$, calculated numerically for the retarded dipole field with $\alpha = 45°$ and $\zeta = 43°$. In agreement with BCW91, its center lags the phase zero by $2r_{\mathrm{n}}$ rad $= 1.14°$, and there is no discernible sign of the sweepback effect (see Section 2).

If the central parts of the pulse profile originate from much lower radial distance r than the edge, and if $r \ll 0.01 R_{\mathrm{lc}}$, the central parts of the PA curve do not exhibit any appreciable shift and nearly follow the undisturbed S-curve of Radhakrishnan & Cooke. The solid line which nearly passes through the $(0,0)$ point in Fig. 6b has been calculated for the emission from the last open magnetic field lines of the retarded dipole for the same α and ζ as above. The corresponding radial distance of the radio emission as a function of phase ϕ is shown in panel a of Fig. 6. Within the central parts of the PA curve, the emission altitude is negligibly

small and the PA curve nearly follows the undisturbed S-swing (dotted line in Fig. 6b).

Thus, in the case when the central parts of the profile are emitted from much lower altitudes than the outer edge of the profile, the PA swing practically does not undergo the delay by $2r_{\rm n}$. The misalignment formula (19) then becomes

$$\Delta\Phi \approx 2r_{\rm n} - Fr_{\rm n}^{1/2} \qquad (22)$$

and is illustrated in Fig. 7 with the same layout as Fig. 4. One can see that in the considered case, the shift is much smaller than the shift predicted by the standard delay-radius formula (eq. 2, thick dashed line in Fig. 7). For a typical phase shift $\Delta\Phi \sim 0.3°$ eq. (2) underestimates r by an order of magnitude. The range of altitudes for which the shift is negative is much larger than in the case with the constant emission altitude (eq. 19, Fig. 4).

In the considered case of the low-altitude emission within the profile center, the determination of the radial distance of radio emission $r_{\rm n}$ is performed as before (Section 3.2) with the only difference in that eq. (20) should be replaced by the inverse of eq. (22), ie. Fig. 7 should be used instead of Fig. 4. Even allowing for the low-altitude origin of the central parts of the pulse profile, for B0525+21 at 430 MHz we still have $r_{\rm n} < r_{\rm geo}/R_{\rm lc}$. Apparently, either the radio beam of this pulsar does not fill in the open volume or other effects are important. These may include the overestimate of dipole inclination and/or $|\beta|$, the broadening of the observed pulse width due to the low energy of radio emitting electrons (all of which lead to the overestimate of $r_{\rm geo}$) or refraction, eg. Lyubarski & Petrova (1998). However, our radial distance $r_{\rm n} \simeq 7 \cdot 10^{-3}$ underestimates $r_{\rm geo}/R_{\rm lc}$ by a factor of 2.5 whereas the original delay-radius formula underestimates it by a much larger factor of 13.

5.   Conclusions

The rotational distortions of the vaccum dipole have twofold effect: in addition to the small changes of the local direction of the magnetic field, the region of the open magnetic field lines undergoes a strong distortion.

The change of the local direction of $\vec{B}$ is second order in $r_{\rm n}$. We find, however, that it is symmetrical with respect to the $(\vec{\Omega}, \vec{\mu})$ plane. The largest asymmetrical change of $\vec{B}$ direction is much smaller – third order in $r_{\rm n}$, in agreement with Shitov's estimate.

The displacement of the open volume shifts the pulse window toward later phases with respect to the center of the position angle curve. The shift has the magnitude of the order of $r_{\rm n}^{1/2}$. The open volume shift modifies the delay-radius relation if the center of the pulse profile is determined as the midpoint between the outer edges of the pulse profile, which are

assumed to lie close to the outer boundary of the open volume. At low altitudes, where effects of aberration and propagation time delays are small, the open volume shift dominates and may result in the center of the PA curve *preceding* the center of the profile (negative $\Delta\Phi$). A majority of pulsars exhibits positive $\Delta\Phi$ which means that the radio emission altitudes typically exceed $\sim 10^{-2}R_{\mathrm{lc}}$.

The radii derived with the misalignment formula exceed those derived with the original delay-radius relation by a factor which increases quickly with decreasing altitude (and $\Delta\Phi$). This explains the trend of the delay-radius relation to predict emission radii smaller than the geometrical radii. The underestimate may also be produced/enhanced by the low-altitude emission within the central parts of the pulse profile. When both these effects work together, the standard delay-radius relation may underestimate r by an order of magnitude even for the relatively large phase shifts ($\Delta\Phi \sim 0.3°$).

The influence of the open volume shift on the method based on the core-cone shift (eq. 3) is difficult to assess, because the locations of the conal maxima do not need to follow the open boundary of the open volume. If they did, eq. (3) would have to be replaced with $\Delta\phi_{DRH} \approx 2r_{\mathrm{n}} - Fr_{\mathrm{n}}^{1/2}$. The influence of the open volume shift on the geometrical method is small because the rotation increases the transverse size of the open volume insignificantly (by a factor smaller than ~ 1.2, cf. Fig. 2).

The discussed distortion of the open volume is generated by a high-order effect which was being neglected for years on the basis that its "local magnitude" at low altitudes is small ($\sim r_{\mathrm{n}}^2$). The actual importance of this effect appears to be much larger than that. This suggests that other "high-order" effects, eg. the longitudinal polar cap currents, of magnitude $\sim r_{\mathrm{n}}^{3/2}$, or the inertia of electrons, may be a lot more significant than their low altitude magnitude suggests. The toroidal currents due to the corotation of the charge-filled magnetosphere ($\sim r_{\mathrm{n}}^2$) have been shown to notably modify the shape of the open volume, however, in a way which is symmetrical with respect to the $(\vec{\Omega}, \vec{\mu})$ plane (cf. fig. 4.11 in Beskin et al. 1993).

A.   Retarded vs static dipole

In the reference frame with $\hat{z} \parallel \vec{\Omega}$ the "retarded" field $\vec{B}_{\mathrm{ret}}$ of the vacuum magnetic point dipole with the magnetic moment given by eq. (5) has the following cartesian components:

$$
B_{\mathrm{ret},x} = \frac{\mu}{r^5}\Big\{ 3xz\cos\alpha + \sin\alpha \Big(\big[(3x^2 - r^2) + 3xyr_{\mathrm{n}} + (r^2 - x^2)r_{\mathrm{n}}^2\big]\cos(\Omega t - r_{\mathrm{n}}) +
$$
$$
\big[3xy - (3x^2 - r^2)r_{\mathrm{n}} - xyr_{\mathrm{n}}^2\big]\sin(\Omega t - r_{\mathrm{n}}) \Big)\Big\} \tag{A1}
$$

$$
B_{\mathrm{ret},y} = \frac{\mu}{r^5}\Big\{ 3yz\cos\alpha + \sin\alpha \Big(\big[3xy + (3y^2 - r^2)r_{\mathrm{n}} - xyr_{\mathrm{n}}^2\big]\cos(\Omega t - r_{\mathrm{n}}) +
$$
$$
\big[(3y^2 - r^2) - 3xyr_{\mathrm{n}} + (r^2 - y^2)r_{\mathrm{n}}^2\big]\sin(\Omega t - r_{\mathrm{n}}) \Big)\Big\} \tag{A2}
$$

$$
B_{\mathrm{ret},z} = \frac{\mu}{r^5}\Big\{ (3z^2 - r^2)\cos\alpha + \sin\alpha \Big(\big[3xz + 3yzr_{\mathrm{n}} - xzr_{\mathrm{n}}^2\big]\cos(\Omega t - r_{\mathrm{n}}) +
$$
$$
\big[3yz - 3xzr_{\mathrm{n}} - yzr_{\mathrm{n}}^2\big]\sin(\Omega t - r_{\mathrm{n}}) \Big)\Big\} \tag{A3}
$$

It can be derived by any of the methods described in Yadigaroglu (1997), Arendt & Eilek (1998), or CRZ2000. Also, it can be obtained by taking the limit of $R_{\mathrm{ns}}/R_{\mathrm{lc}} \ll 1$ in the solution of Deutsch (1955). For any position $\vec{r}_0$, time t_0 and time interval Δt it holds that

$$
\vec{B}_{\mathrm{ret}}\left(t_0 + \Delta t, R_z(\Omega\Delta t)\vec{r}_0\right) = R_z(\Omega\Delta t)\vec{B}_{\mathrm{ret}}\left(t_0, \vec{r}_0\right), \tag{A4}
$$

where $R_z(\omega)\vec{r}$ represents the rotation of the vector $\vec{r}$ by the angle ω around the $\hat{z}$ axis. Thus, the dependence on the time t only reflects the rigid rotation of the pattern of distorted magnetic field lines around the $\hat{z}$ axis with the angular velocity $\Omega\hat{z}$. The magnetic field $\vec{B}_{\mathrm{st}}$ of the static-shape dipole associated with the same magnetic moment $\vec{\mu}$ (eq. 5) is given by the same set of equations (A1 – A3) with $r_{\mathrm{n}} = 0$.

Using eqs. (A1 – A3) with $t = 0$ it can be immediately shown that the difference $\Delta\vec{B} = \vec{B}_{\mathrm{ret}} - \vec{B}_{\mathrm{st}}$ is given by eqs. (6 – 8). Using (4) and (6 – 8) one can find that the angle $\kappa = \arccos(\vec{B}_{\mathrm{ret}} \cdot \vec{B}_{\mathrm{st}}/(B_{\mathrm{ret}}B_{\mathrm{st}}))$ is given by eq. (9) with f_1, f_2, and f_3 given by

$$
f_1 = h_1 - g_1^2, \qquad f_2 = h_2 - 2g_1g_2 \tag{A5}
$$

and

$$
f_3 = 2g_1^3 + h_3 - g_2^2 - 2g_1(g_3 + h_1) \tag{A6}
$$

with

$$
g_1 = \frac{1}{2}c_1\left[\left(5\frac{x^2}{r^2} - 1\right)\sin\alpha + 5\frac{x^2}{r^2}\cos\alpha\right] \tag{A7}
$$

$$
g_2 = -2c_1\left[\frac{xy}{r^2}\sin\alpha + \frac{y^2}{r^2}\cos\alpha\right] \tag{A8}
$$

$$g_3 = \frac{1}{8} c_1 \left[\left(3 - 7\frac{x^2}{r^2} \right) \sin \alpha - 7\frac{x^2}{r^2} \cos \alpha \right] \tag{A9}$$

$$h_1 = \frac{1}{4} c_1 \sin \alpha \left(3\frac{x^2}{r^2} + 1 \right) \tag{A10}$$

$$h_2 = -\frac{2}{3} c_1 \sin \alpha \frac{x}{r}\frac{y}{r} \tag{A11}$$

$$h_3 = -\frac{1}{8} c_1 \sin \alpha \left(\frac{x^2}{r^2} - \frac{5}{9} \right) \tag{A12}$$

$$c_1 = \frac{\sin \alpha}{1 + 3 \left(xr^{-1} \sin \alpha + zr^{-1} \cos \alpha \right)^2}. \tag{A13}$$

The function f_4 in eq. (15) is equal to

$$f_4 = \frac{1}{2} \left(\frac{\mu}{r^3} \right)^2 \frac{\sin \alpha}{B_{st,x}^2} \frac{y}{r} \left(3\frac{z}{r} \cos \alpha + 4\frac{x}{r} \sin \alpha \right), \tag{A14}$$

where $B_{st,x}$ is given in eq. (13).

The cartesian components of the retarded magnetic field given by eqs. (A1 – A3) can be rewritten into the following spherical components of $\vec{B}_{\text{ret}}$ in the reference frame with $\hat{z} \parallel \vec{\Omega}$:

$$B_{\text{ret},r} = \frac{2\mu}{r^3} \{ \cos \alpha \cos \theta + \sin \alpha \sin \theta \left[r_n \sin \lambda + \cos \lambda \right] \} \tag{A15}$$

$$B_{\text{ret},\phi} = -\frac{\mu}{r^3} \sin \alpha \left[\left(r_n^2 - 1 \right) \sin \lambda + r_n \cos \lambda \right], \tag{A16}$$

$$B_{\text{ret},\theta} = \frac{\mu}{r^3} \{ \cos \alpha \sin \theta + \sin \alpha \cos \theta \left[-r_n \sin \lambda + \left(r_n^2 - 1 \right) \cos \lambda \right] \} \tag{A17}$$

where

$$\lambda = r_n + \phi - \Omega t. \tag{A18}$$

Again, the (spherical) components of $\vec{B}_{\text{st}}$ are given by eqs. (A15 – A18) with $r_n = 0$.

Using eqs. (A15 – A17) in eq. (4) it can be easily shown that

$$\Delta B_r = \frac{\mu}{r^3} \sin \alpha \sin \theta \left[r_n^2 \cos \delta - \frac{2}{3} r_n^3 \sin \delta + O \left(r_n^4 \right) \right] \tag{A19}$$

$$\Delta B_\phi = \frac{\mu}{r^3} \sin \alpha \left[-\frac{1}{2} r_n^2 \sin \delta - \frac{2}{3} r_n^3 \cos \delta + O \left(r_n^4 \right) \right] \tag{A20}$$

$$\Delta B_\theta = \frac{\mu}{r^3} \sin \alpha \cos \theta \left[\frac{1}{2} r_n^2 \cos \delta - \frac{2}{3} r_n^3 \sin \delta + O \left(r_n^4 \right) \right], \tag{A21}$$

where $\delta = \phi - \Omega t$.

REFERENCES

Arendt, P. N., & Eilek, J. A. 1998, ApJ, submitted (astro-ph/9801257)

Beskin, V. S., Gurevich, A. V., & Istomin, Y. N. 1993, "Physics of the Pulsar Magnetosphere", Cambridge University Press, Cambridge

Barnard, J. J. 1986, ApJ, 303, 280

Blaskiewicz, M., Cordes, J. M., & Wasserman, I. 1991, ApJ, 370, 643 (BCW91)

Cheng, K. S., Ruderman, M. A., & Zhang, L. 2000, ApJ, 537, 964 (CRZ2000)

Cordes, J. M. 1978, ApJ, 222, 1006

Deutsch, A. J. 1955, Ann. d'Astrophys., 18, 1

Dyks, J., Rudak, B., & Harding, A. K. 2004a, ApJ, in press (astro-ph/0307251)

Dyks, J., Harding, A. K., & Rudak, B. 2004b, ApJ, in press (astro-ph/0401255)

Everett, J. E., & Weisberg, J. M. 2001, ApJ, 553, 341 (EW2001)

Gangadhara, R. T., & Gupta, Y. 2001, ApJ, 555, 31

Gil, J. 1983, A&A, 127, 267

Gil, J. A., & Kijak, J. 1993, A&A, 273, 563

Gupta, Y., & Gangadhara, R. T. 2003, ApJ, 584, 418

Hibschman, J. A., & Arons, J. 2001, ApJ, 546, 382 (HA2001)

von Hoensbroech, A., & Xilouris, K. M. 1997, A&A, 324, 981

Kapoor, R.C., & Shukre, C.S. 2002, astro-ph/0205429

Kijak, J., & Gil, J. 2002, A&A, 392, 189

Lyne, A. G., & Manchester, R. N. 1988, MNRAS, 234, 477

Lyubarskii, Y. E., & Petrova, S. A. 1998, A&A, 333, 181

Mitra, D., & Li, X. H. 2004, A&A, in press

Mitra, D., & Rankin, J. M. 2002, ApJ, 577, 322

Radhakrishnan, V., & Cooke, D. J. 1969, Astrophys. Lett., 3, 225

Rankin, J. M. 1990, ApJ, 352, 247

Rankin, J. M. 1993, ApJ, 405, 285

Romani, R. W. & Yadigaroglu, I.-A., 1995, ApJ, 438, 314

Shitov, Yu., P. 1983, Sov. Astron, 27, 314

Shitov, Yu., P. 1983, Sov. Astron, 29, 33
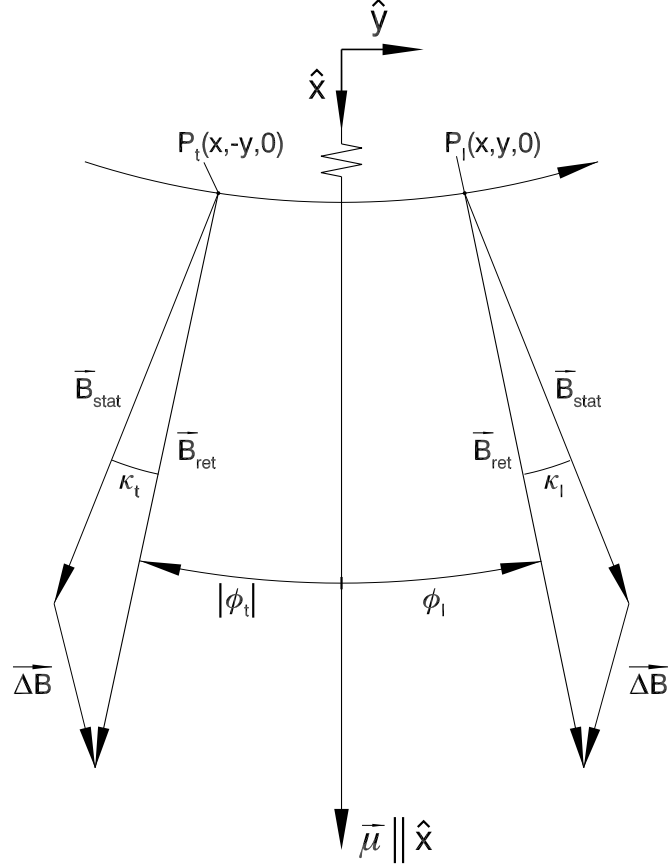
Yadigaroglu, I.-A. 1997, Ph.D. thesis, Stanford University

Fig. 1.— The influence of rotation on the local direction of the magnetic field. The vectors of $\vec{B}_{\mathrm{ret}}$ and $\vec{B}_{\mathrm{st}}$ are shown for two points in the equatorial plane of the orthogonal rotator ($\alpha = 90°$). The points are located symmetrically with respect to the $(\vec{\Omega}, \vec{\mu})$ plane (the plane is orthogonal to the page and contains $\hat{x}$). The rotation is to the right and it is assumed that $x \gg y$ (region near the dipole axis) and $x \ll R_{\mathrm{lc}}$. With accuracy of r_{n}^2, the retarded field $\vec{B}_{\mathrm{ret}}$ is symmetrical with respect to the $(\vec{\Omega}, \vec{\mu})$ plane, ie. $\kappa_{\mathrm{l}} = \kappa_{\mathrm{t}}$ and $|\phi_{\mathrm{t}}| = \phi_{\mathrm{l}}$. More precisely, $\kappa_{\mathrm{l}} = \kappa_{\mathrm{t}} + O(r_{\mathrm{n}}^3)$ and $\phi_{\mathrm{t}} = -\phi_{\mathrm{l}} - O(r_{\mathrm{n}}^3)$, ie. $\kappa_{\mathrm{t}} < \kappa_{\mathrm{l}}$ and $|\phi_{\mathrm{t}}| > \phi_{\mathrm{l}}$.
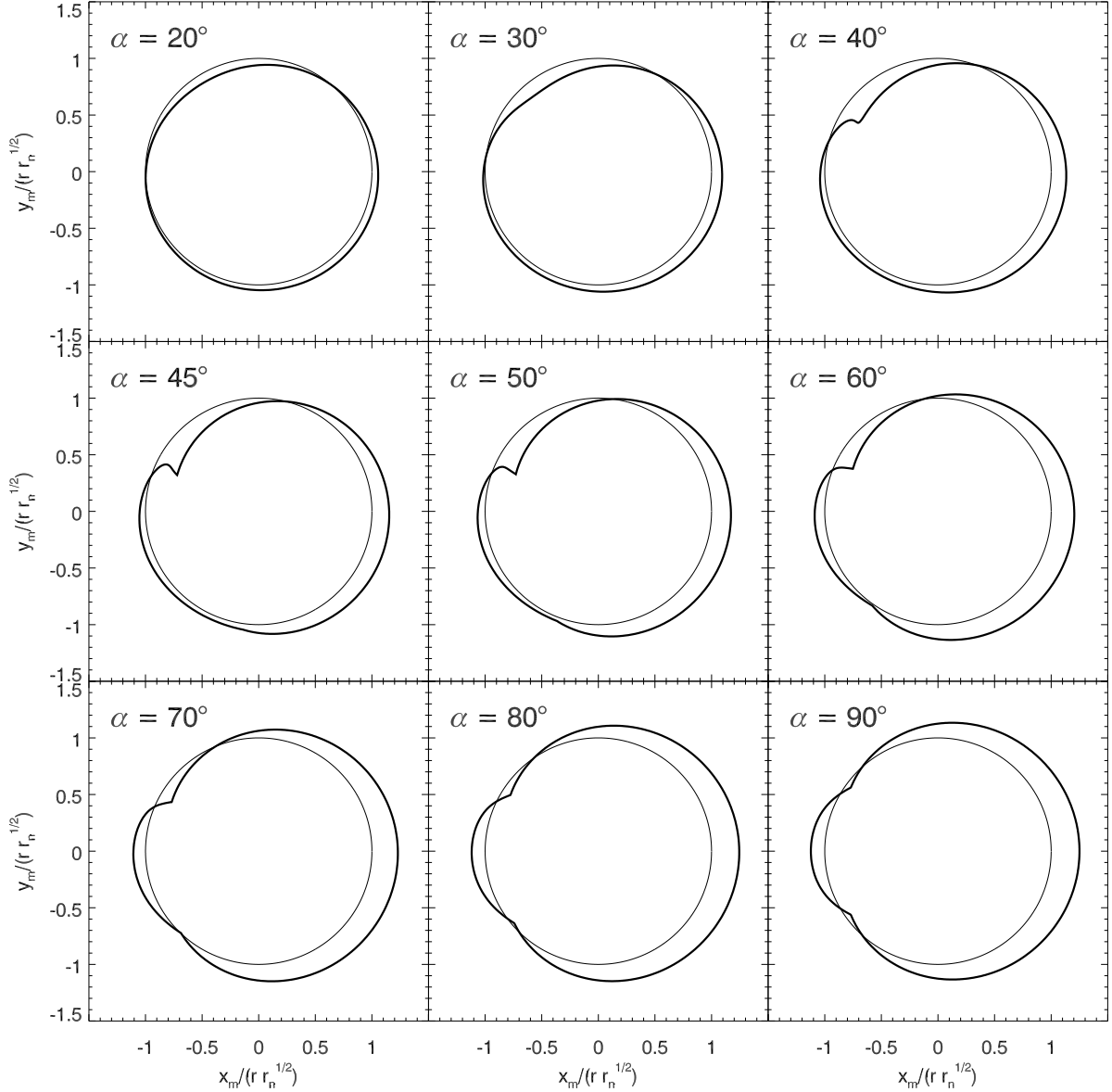
Fig. 2.— Crossections of the open volume with the star-centered sphere of radius $r \ll R_{\mathrm{lc}}$ calculated for the retarded dipole field $\vec{B}_{\mathrm{ret}}$ (thick solid). The circles have radius of $r r_{\mathrm{n}}^{1/2}$ and are centered on the magnetic moment $\vec{\mu}$ which protrudes perpendicularly from the page at the center of each panel $((x_{\mathrm{m}}, y_{\mathrm{m}}) = (0, 0))$. The magnetic field $\vec{B}_{\mathrm{ret}}$ which permeates each of the panels is nearly the same as that of the static-shape dipole with the axis parallel to $\vec{\mu}$ (ie. it protrudes from the $(0, 0)$ point too). Rotation is to the left. The backward displacement of the retarded contours with respect to the $(0, 0)$ points (or circles) results in the shift of the center of the pulse profile toward later phases. The shape of the contours does not depend on r and P as long as $r \ll R_{\mathrm{lc}}$ ($P = 1$ s, and $r_{\mathrm{n}} = 0.01$ was assumed in the figure). Their size scales as $r r_{\mathrm{n}}^{1/2}$.
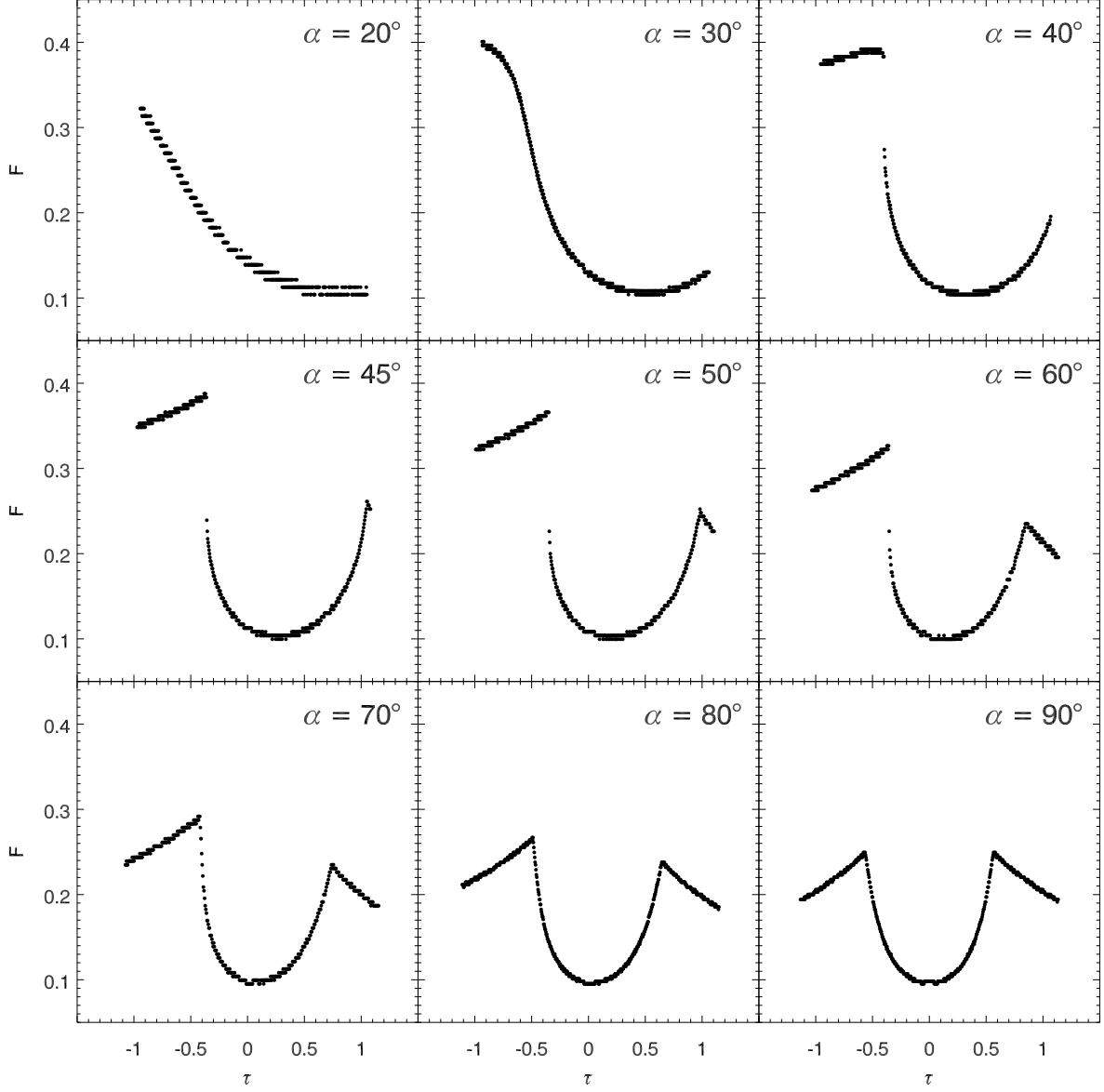
Fig. 3.— The parameter F of eq. 17 as a function of the parameter $\tau = \beta_{\mathrm{x}}/(1.5r_{\mathrm{n}}^{1/2})$ for the same dipole inclinations α as in Fig. 2. Though the results were obtained for $r_{\mathrm{n}} = 0.01$, the curves change little with r_{n}, as long as $r_{\mathrm{n}} \ll 1$.
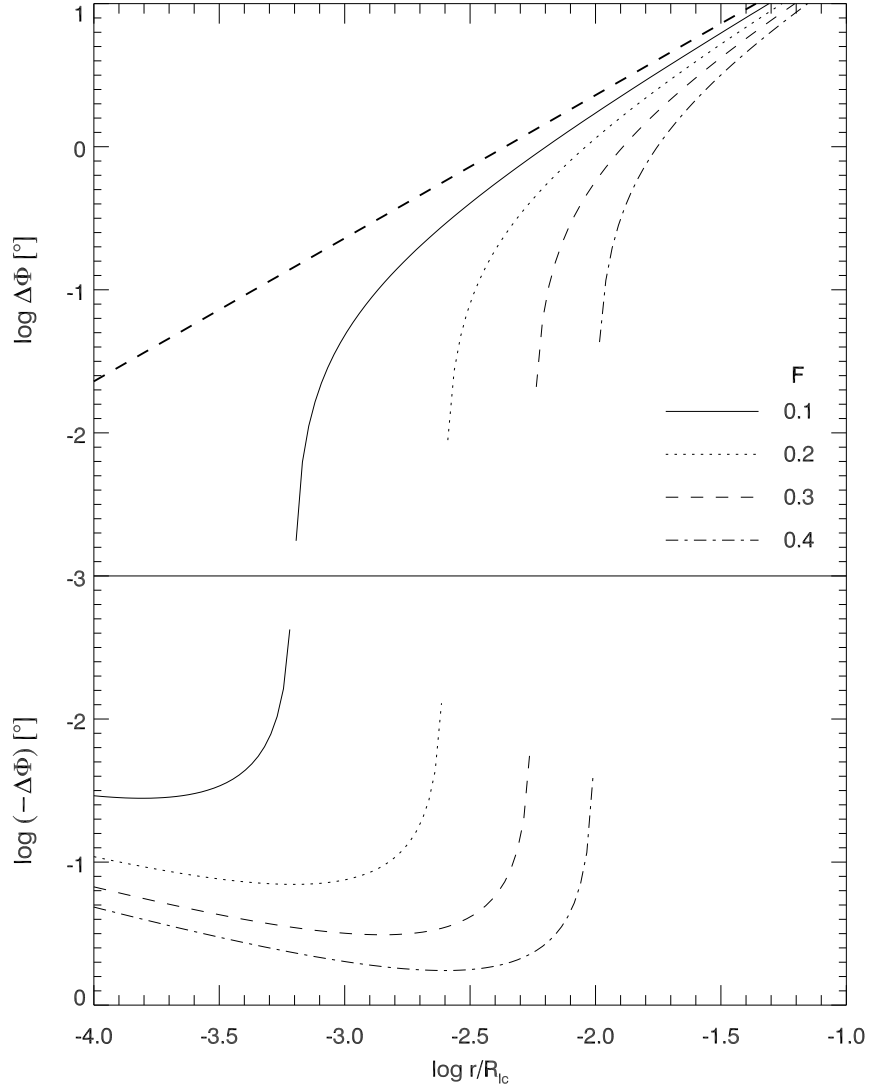
Fig. 4.— The phase shift between the center of the PA curve and the profile center as a function of the radial distance of the radio emission. The four curves show the case with the rotational distortion of the open volume included (eq. 19) and correspond to different values of the parameter F shown in the lower right corner of the upper panel. The thick dashed line presents the original delay-radius relation (eq. 2) which does not include the sweepback effect. In the upper panel the positive shift is shown (the PA curve lags the profile). The lower panel is for the negative shift (the PA curve precedes the pulse profile). Note that the original delay-radius relation significantly underestimates r_n, especially for small $\Delta\Phi$ and r/R_{lc}.
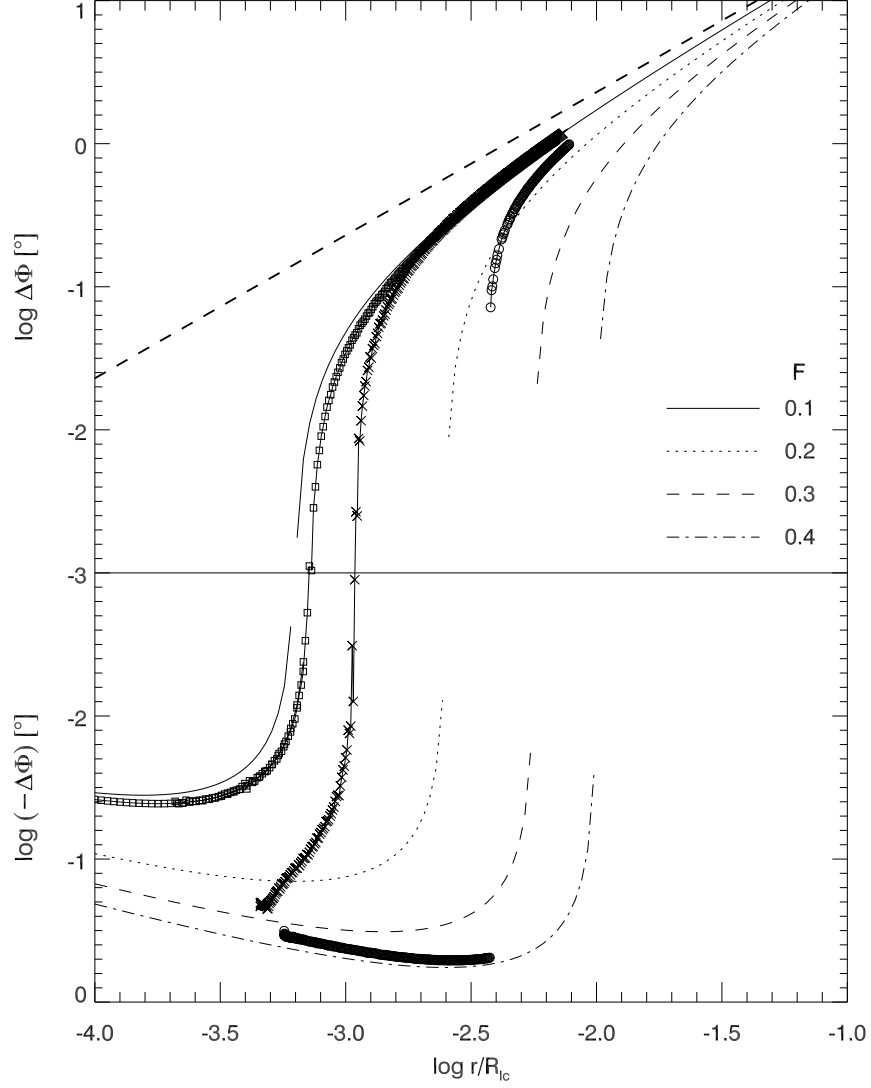
Fig. 5.— Three numerical results for $\alpha = 45°$ (and different viewing angles ζ) overplotted on the curves from Fig. 4. The circles are for the poleward viewing geometry with $\zeta = 43°$ (the curve is broken into two parts, one with positive, and the other with negative $\Delta\Phi$), the crosses are for the equatorward viewing with $\zeta = 47°$, and the squares are for $\alpha = \zeta = 45°$. For more details see text.
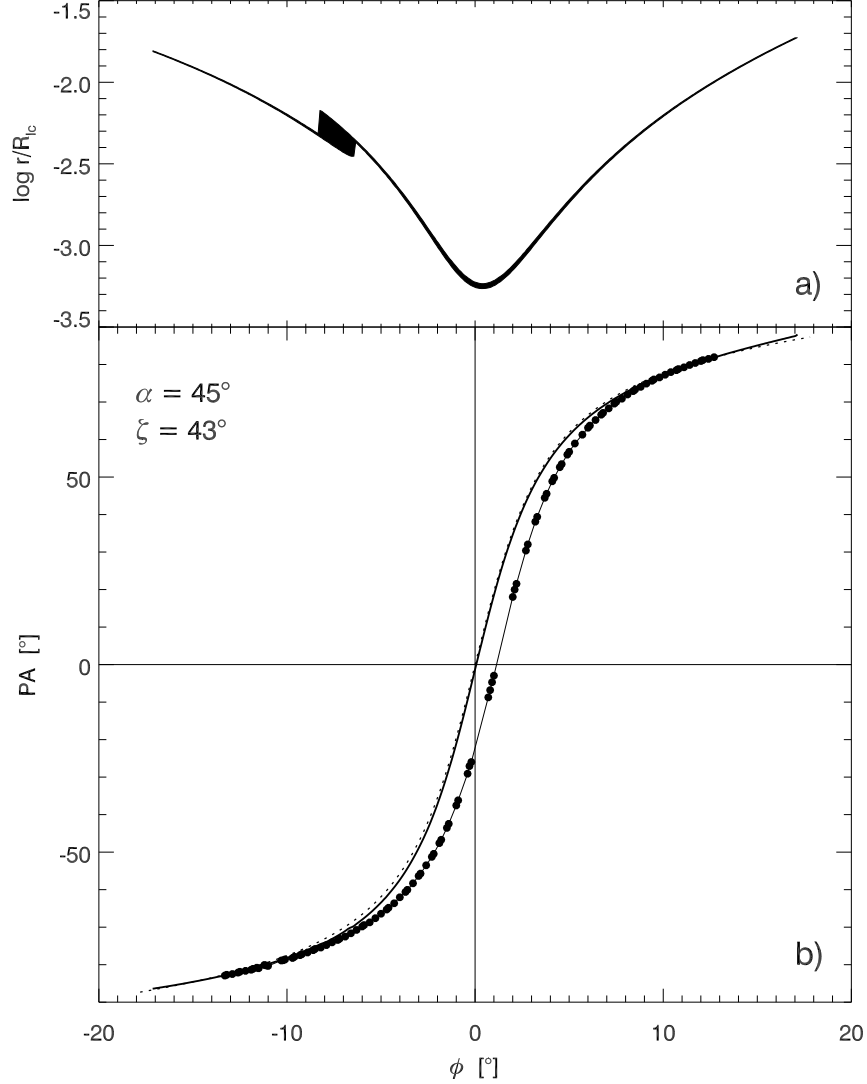
Fig. 6.— Influence of variations of emission altitudes across the pulse profile on the shape of the PA curve. Thin solid line with dots (panel b) presents the position angle curve for emission from the fixed radial distance of $r_n = 0.01$. Its center lags the phase zero by $2r_n$ rad $\approx 1.14°$. The thick solid line in panel b is for the radio emission from the last open field lines, ie. it corresponds to different radial distances shown in panel a. Note that the PA curve for the case of varying r does not exhibit any noticeable lag. The spread in r visible in panel a) near $\phi = -7°$ corresponds to the notch in the open volume which appears for moderate dipole inclinations (cf. Fig. 2, $\alpha = 45°$). The dotted line (nearly overlapping with the thick solid) is the curve of Radhakrishnan & Cooke (1969), undisturbed by the special relativistic effects.
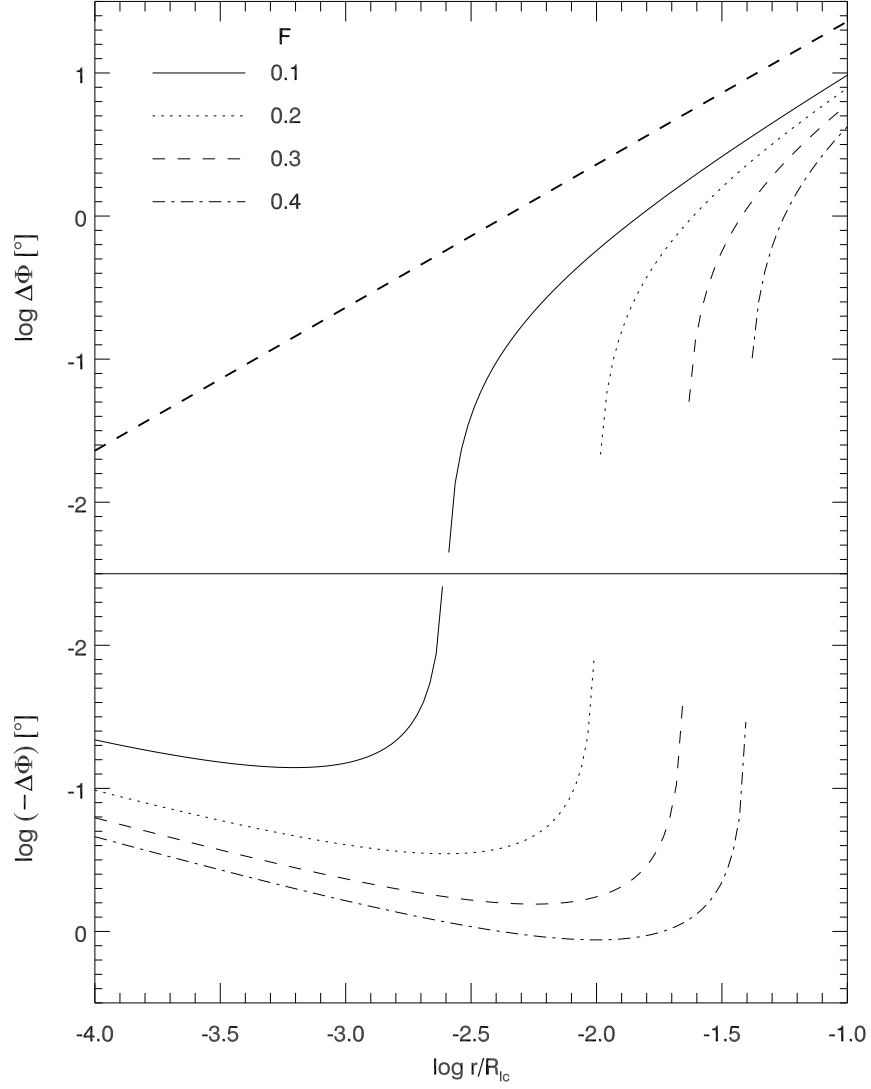
Fig. 7.— Dependence of the shift between the center of the PA curve and the profile center on the radial distance of the radio emission in the case when the central parts of the pulse profile originate from much lower altitude than its edge (ie. for the case marked in Fig. 6 with the thick solid line). The layout is the same as in Fig. 4. Note the increased divergence from the original delay-radius relation (thick dashed line).